From the results presented in Tables 2 and 3, it is found that the theoretical results on strength prediction are conservative and quite acceptable, while the prediction of the deflection is not as good.

REFERENCES

1. Takeda, N., R. L. Sierakowski, and L. E. Malvern. "Microscopic Observations of Cross Sections of Impacted Composite Laminates," *Composite Technology Review*, 4:40–44 (1982).
2. Joshi, S. P. and C. T. Sun. "Impact Induced Fracture in a Laminated Composite," *J. Composite Materials*, 19:51–66 (1985).
3. Rhodes, M. D., J. G. Williams, and J. A. Starnes. "Low-Velocity Impact Damage in Graphite-Fiber Reinforced Epoxy Laminates," *Polymer Composites*, 2(1):36–44 (1981).
4. Gu, Z. L. and C. T. Sun. "Characterization of Impact Damage in an SMC-R50 Composite," in *1983 Advances in Aerospace Structure, Materials and Dynamics*. U. Yuceoglu, R. L. Sierakowski, and D. A. Glasgow, eds. The American Society of Mechanical Engineers, pp. 75–80 (1983).

Composite Box Beam Analysis: Theory and Experiments

O. A. BAUCHAU
Rensselaer Polytechnic Institute
Department of Mechanical Engineering
Aeronautical Engineering and Mechanics
Troy, New York 12180

B. S. COFFENBERRY
Material Sciences Corporation
Spring House, Pennsylvania 19477

L. W. REHFIELD
Georgia Institute of Technology
School of Aerospace Engineering
Atlanta, Georgia 30332

ABSTRACT

Beam theory is widely used as a first approximation in numerous structural applications. When applied to composite beams, the accuracy of beam theory becomes questionable because (1) the shearing and warping deformations become significant, as the shearing stiffness of composite laminates is often very low, and (2) several elastic couplings can occur that strongly influence the behavior of composite beams. The torsional behavior of thin-walled composite beams has important implications for aeronautical structures and is deeply modified by the above non-classical effects. This paper presents two comprehensive analysis methodologies for composite beams and describes experimental results obtained from a thin-walled, rectangular cross-sectional beam. The theoretical predictions are found in good agreement with the observed twist and strain distributions. Out-of-plane torsional warping of the cross-section is found to be the key factor for an accurate modeling of the torsional behavior of such structures.

1. INTRODUCTION

IN NUMEROUS AERONAUTICAL APPLICATIONS, THE STRUCTURAL DESIGNER often uses Timoshenko beam theory as a preliminary design tool or as a means of conducting design impact assessments. In other cases, like helicopter blade stability analysis, beam theory is the basis for the structural modeling. Currently, composite beams are treated in a manner similar to that used for metal beams. The only distinguishing feature is that the effective extensional modulus

0731-6844/87/01 0025-11 $4.50/0

is not related to the shear modulus. This approach does not permit the description of general composite lay-ups, and its accuracy is questionable in view of the following facts:

(a) The use of laminated composite materials results in significant shearing and warping of the beam. These effects are far more pronounced for highly anisotropic composites than for metals, as they are proportional to the ratio of the extensional modulus to the shearing modulus. This ratio is typically 2.6 for metals, but it could be an order of magnitude larger for composites.
(b) The proper tailoring of composite lay-ups results in elastic couplings, e.g., bending-twisting, or extension-twisting couplings which strongly influence the overall behavior of the beam as well as the strain distributions. Such couplings are not appropriately modeled with standard beam theory.

This paper will briefly review two comprehensive analysis methodologies for composite beams. Both analyses assume the cross-section of the beam to be infinitely rigid in its own plane, but the modeling of the out-of-plane warping behavior is different in the two approaches. Next, an experimental program will be described briefly, and the measured displacements and strain distributions will be compared to theoretical prediction. This comparison will focus on the torsional behavior of the beam, as it is most critically affected by non-classical effects.

2. GEOMETRY OF THE BEAM

A thin-walled box beam with closed cross-sections will be considered (see Figure 1). The contour of the cross-section (denoted C) is a parametric function of the variable s, and the variable z runs along the span of the beam. Each section is assumed to be infinitely rigid in its own plane, implying (1) that the inplane displacements of the section can be represented by three rigid body motions $U(z)$, $V(z)$, and $\theta(z)$, respectively the two translations and the rotation of the section, and (2) that any applied transverse load only induces membrane stresses in the structure, namely the axial stress flow n, and the shear stress flow q. For thin-walled beams these two stress flows are uniform across the wall thickness and the other stress components are assumed to be negligible.

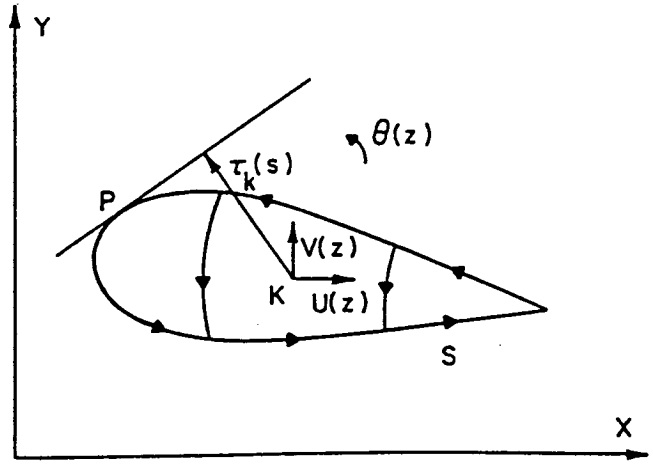

Figure 1. Geometry of a typical cross-section.

Using Classical Lamination Theory [1], the stress flow-strain relationships are:

$$\begin{bmatrix} n \\ n_t \\ q \end{bmatrix} = \begin{bmatrix} A_{11} & A_{12} & A_{16} \\ & A_{22} & A_{26} \\ & & A_{66} \end{bmatrix} \begin{bmatrix} \epsilon \\ \epsilon_t \\ \gamma \end{bmatrix} \tag{1}$$

where A_{ij} are the components of the in-plane stiffness matrix that can be calculated from material properties and composite lay-up definition; ϵ and γ are the axial and shearing strain components. The hoop stress flow n_t being negligible, the hoop strain ϵ_t can be eliminated, yielding

$$\begin{bmatrix} n \\ q \end{bmatrix} = \begin{bmatrix} A_{nn} & A_{nq} \\ & A_{qq} \end{bmatrix} \begin{bmatrix} \epsilon \\ \gamma \end{bmatrix} \tag{2}$$

where $A_{nn} = A_{11} - A_{12}^2/A_{22}$; $A_{qq} = A_{66} - A_{26}^2/A_{22}$; $A_{nq} = A_{16} - A_{12}\,A_{26}/A_{22}$. When the material is isotropic, or orthotropic with the axes of orthotropy parallel to the axis of the beam and the tangent to C, respectively, $A_{16} = A_{26} = 0$, resulting in $A_{nq} = 0$. A non-vanishing A_{nq} is responsible for extension-shearing coupling of the laminate, and results in elastic couplings for the beam.

Finally the strain-displacements relationships are easily found as

$$\epsilon = \frac{\partial w}{\partial z}$$

$$\gamma = \frac{\partial w}{\partial s} + U' \frac{dx}{ds} + V' \frac{dy}{ds} + \theta' r_k \tag{3}$$

where w is the axial displacement, r_k the normal projection of the position vector (see Figure 1), and $(\ )'$ means derivative with respect to z. The strain energy is now

$$U = \frac{1}{2} \int_o^L \int_C (A_{nn}\,\epsilon^2 + A_{qq}\,\gamma^2 + 2Anq\,\epsilon\,\gamma)\,ds\,dz$$

where L is the span of the beam.

3. THE SAINT-VENANT WARPING APPROACH

This first approach is based on the following assumed displacement field:

$$u(s,z) = U(z) \qquad -y\,\theta(z) \tag{5}$$

$$v(s,z) = V(z) \qquad +x\,\theta(z) \tag{6}$$

$$w(s,z) = W(z) + xX(z) + yY(z) + \psi(s)\theta'(z) \tag{7}$$

where u, v, and w are the displacement components in the x, y, and z directions respectively; X and Y are the rotations of the cross-section. $\psi(s)$ is the St. Venant torsion related warping function [2]. The resulting strain field is

$$\epsilon = W' + xX' + yY' + \psi\theta''$$

$$\gamma = (X + U')\frac{dx}{ds} + (Y + V')\frac{dy}{ds} + \left(\frac{d\psi}{ds} + r_k\right)\theta' \tag{8}$$

The strain energy can be evaluated by placing Equations (8) into (4) and integrating over the cross-section. The governing differential equations are then obtained by minimizing the total potential energy of the beam. The details of the analysis, and the governing equations are reported in [3]. The kinematic assumptions underlying this approach are (1) the cross-section does not deform in its own plane [implying (5) and (6)] and (2) the out-of-plane deformation of the cross-section is restricted to the St. Venant torsion related warping [implying (7)]. The kinematic variables are U, V, W, X, Y, and θ, respectively the three translations and the three rotations of the cross-section.

4. THE EIGENWARPING APPROACH

In this second approach, the assumed in-plane displacement field is identical to that of the previous approach, i.e. (5) and (6) still hold, but the axial displacement field is now written as:

$$w(s,z) = W(z) + xX(z) + yY(z) + \sum_i W_i(s)F_i(z) \tag{9}$$

where $W_i(s)$ are the eigenwarping modes of the cross-section, and $F_i(z)$ are generalized coordinates. The eigenwarping modes are a function of the cross-sectional geometry and stiffness distribution; their detailed derivation is given in [4]. Relation (9) is in fact a series expansion of the axial displacements in terms of the orthogonal eigenwarping functions. This means that arbitrary displacement

fields can be represented. The strain field now becomes:

$$\epsilon = W' + xX' + yY' + \sum_i W_i(s)F_i'(z)$$

$$\gamma = (X + U')\frac{dx}{ds} + (Y + V')\frac{dy}{ds} + r_k\theta' + \sum_i \frac{dW_i}{ds}F_i \tag{10}$$

Placing (10) into (4) and integrating over the cross-section yields the strain energy expression and the governing equations are then obtained by minimizing the total potential energy of the structure. Reference 4 gives the details of the derivation as well as the final governing equations. The only assumption in this approach is that the cross-section does not deform in its own plane. The kinematic variables are U, V, W, X, Y, θ, and one generalized coordinate F_i for each eigenwarping mode included in the analysis. It has been shown in [4] that retaining the few first terms only in the series expansion (9) gives a converged solution. The results presented in this paper were obtained using three torsion related eigenwarping modes.

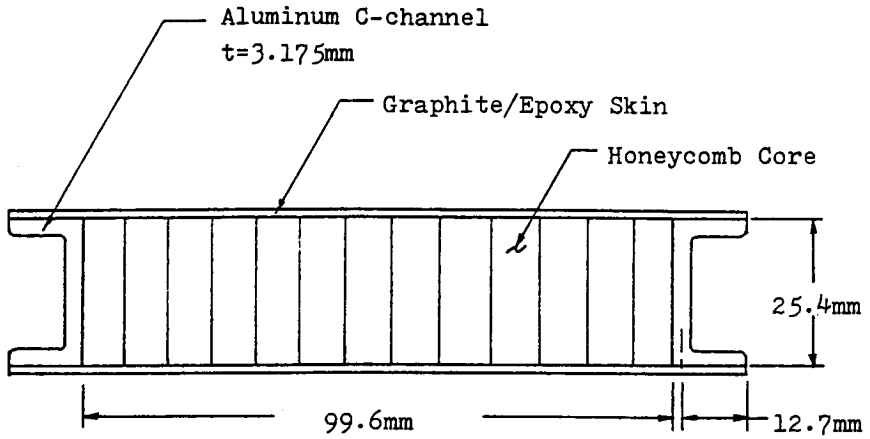

Figure 2(a). *Cross-section of the beam.*

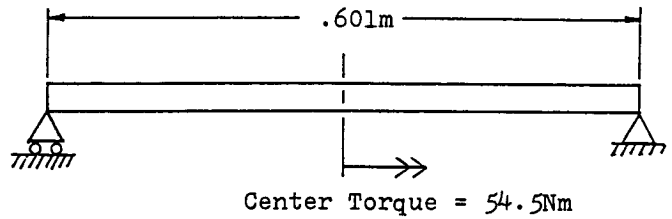

Figure 2(b). *Schematics of test configuration.*

5. DESCRIPTION OF THE EXPERIMENTAL SETUP

In order to validate the above analysis methodologies a simple test was designed, consisting of a thin-walled beam with a rectangular cross-section (see Figure 2a and b). The upper and lower panels of the beam are graphite/epoxy laminated plates with aluminum C-channels forming the webs. The flanges of the channel are attached to the laminates with resin and stainless steel fasteners. The panels are stabilized with an aluminum honeycomb core (Hexcel ⅛″-5052-.0015″). The graphite/epoxy system consists of Union Carbide Thornel T-300 fibers impregnated with Fiberite 948A1, 250°F cure epoxy resin. The following ply properties of this material were obtained from tensile test coupons:

$$E_L = 134 \pm 5.5 \text{ GPa}; \; E_T = 8.46 \pm 0.1 \text{ GPa}; \; G_{LT} = 5.00 \pm 0.1 \text{ GPa}; \; \nu_{LT} = 0.29$$

Two laminate configurations were considered in this study. The first configuration (referred to as the "balanced beam"), uses $[0_2, \pm 15]_s$ lay-ups for both upper and lower panels (the 0° direction is parallel to the beam axis). In this case, one axis of orthotropy of the laminate is along the beam axis, so that no elastic couplings are present. For the second configuration (the "unbalanced beam"), the same laminate was used but its axis of orthotropy was rotated 15° with respect to the beam axis, resulting in a $[15_2, 30, 0]_s$ lay-up. The relevant stiffness coefficients of these laminates are found from ply properties and relation (2):

$$A_{nn} = 144.2 \; 10^6\text{N/m}, \; A_{qq} = 10.24 \; 10^6\text{N/m}, \text{ and } A_{nq} = 0.0$$

for both panels of the balanced beam, whereas

$$A_{nn} = 119.2 \; 10^6\text{N/m}, \; A_{qq} = 14.05 \; 10^6\text{N/m}, \text{ and } A_{nq} = \pm 22.41 \; 10^6\text{N/m}$$

for the unbalanced configuration. The ± sign of A_{nq} corresponds to the lower and upper skins, respectively.

In the test setup, each end of the beam was simply supported, i.e., transverse displacements and twist were constrained, but cross-sectional rotations and warping displacements were free. Loading was applied as follows: first, a mid-span concentrated transverse load P was applied at the axis of the beam, and then the same load was applied at a distance d from that axis. The displacements and strain distributions corresponding to an applied center torque Pd were then obtained by subtracting the corresponding distributions for these two loading cases.

Two dial gages were placed at center span, each 0.33 m away from the beam axis. The differential dial gage reading yielded an accurate measurement of beam center twist. Three strain gage rosettes located at 45 percent span were used to measure both axial and shear strain distributions across the width of the upper graphite/epoxy skin. One additional rosette was placed at 25 percent span. Figure 3 shows the strain gage arrangement. The instrumentation was identical for both balanced and unbalanced beams.

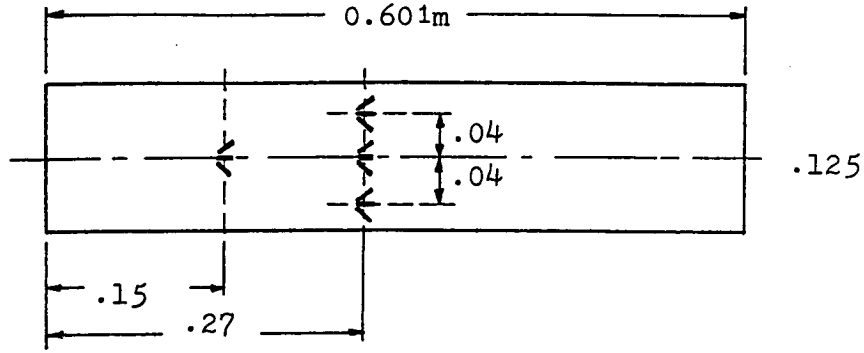

Figure 3. *Location of the strain gage rosettes on the upper graphite/epoxy skin.*

6. COMPARISON OF EXPERIMENTAL RESULTS AND THEORETICAL PREDICTIONS

The experimental results are now presented together with the theoretical predictions of the St. Venant warping and eigenwarping approaches. The comparison also includes Bernoulli Beam Theory [4] and St. Venant Beam Theory [4], which is the standard Beam Theory. Table 1 lists the center twists for the balanced and unbalanced beams, under a center torque of 54.5 Nm. The experimental result corresponds to the average center twist of the two replicates. It is well known that Bernoulli Beam Theory grossly overestimates the torsional stiffness of the beam. In this case, the center twist is 86 percent in error. Standard beam theory (labeled St. Venant), overestimates the center twist by 25 percent, as this solution ignores the stiffening effect of the center span warping constraint inherent to the symmetry of the test configuration. The predictions of the two proposed methodologies are found to be in very close agreement with the experimental measurements. The same trends appear for the unbalanced beam, where excellent correlation is again observed between experimental results and the proposed analyses.

We now turn our attention to the strain distributions in the upper skin of the beam, at 45 percent span, as shown in Figure 4 for the balanced configuration. It is important to note that standard beam theory predicts no axial strain, whereas

Table 1. Comparison of the center twists for the balanced and unbalanced beams under 54.5 Nm center torque (in 10^{-3} rad).

	Balanced Beam		Unbalanced Beam	
Experiment	5.14		4.80	
Bernoulli	0.706	(−86%)	0.724	(−85%)
St. Venant Warping	4.48	(−13%)	4.49	(−6.5%)
Eigenwarping	4.55	(−11%)	4.56	(−5%)
St. Venant	5.67	(+10%)	5.55	(16%)

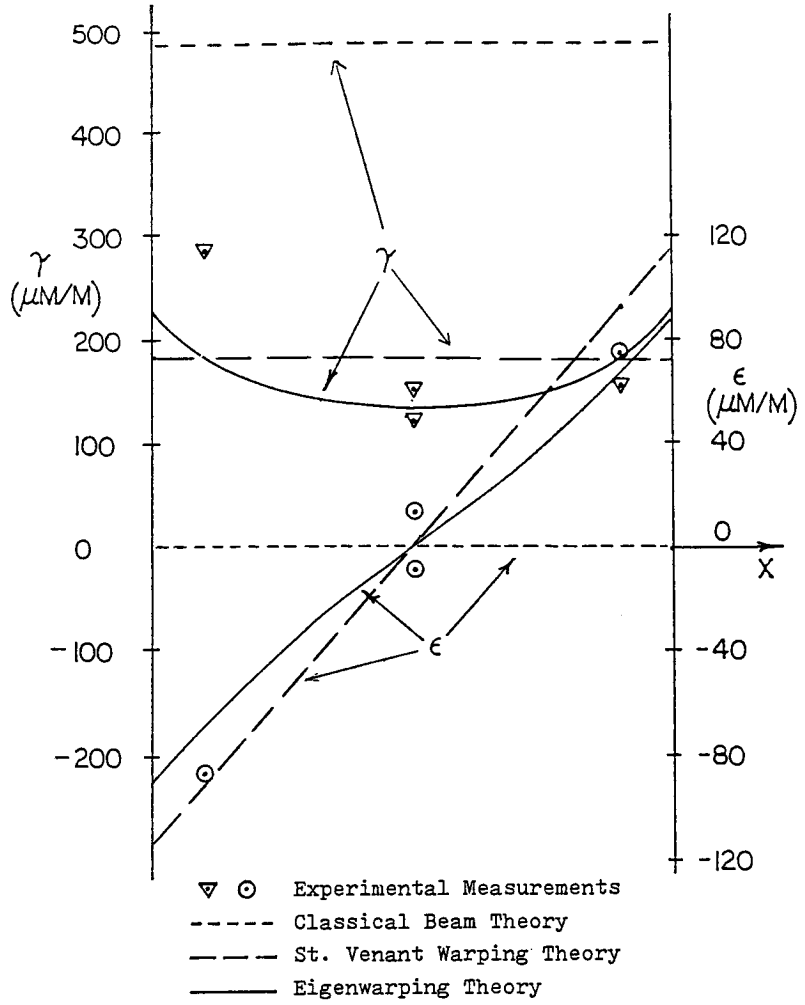

Figure 4. *Strain distributions in the upper skin of the balance beam, at 45% span.*

the experimental measurements show large axial strains near the corner of the cross-section. This axial strain distribution is accurately predicted by both proposed analyses. Considering now the shearing strain distribution, both proposed solutions and the experimental results indicate a level of about 180 microstrains rather than a 500 microstrain level for standard beam theory. It is interesting to note that the St. Venant warping approach predicts a uniform shearing strain across the width of the panel, that averages the distribution predicted by the Eigenwarping approach. Similar trends are observed in Figure 5 which shows the strain distributions for the unbalanced beam configuration.

Finally, the spanwise distribution of the shearing strain at mid-width of the upper skin will be analyzed. Figure 6 shows the experimental results at 25 percent and 45 percent span, along with the various theoretical predictions. Standard beam theory predicts a uniform shear strain distribution, since the torque is uniform along the span. However, the warping constraint at midspan causes a drastic redistribution of the shearing strain, as indicated by the experimental results and both proposed analyses, which are all found in very close agreement. The corresponding results for the unbalanced beam are shown in Figure 7.

7. DISCUSSION AND CONCLUSIONS

The above results clearly indicate that Standard Beam Theory may lead to erroneous predictions of the torsional behavior of thin-walled beams made of anisotropic, laminated composites. The test specimens used in the experimental program were purposely designed to enhance nonclassical effects, as the aspect

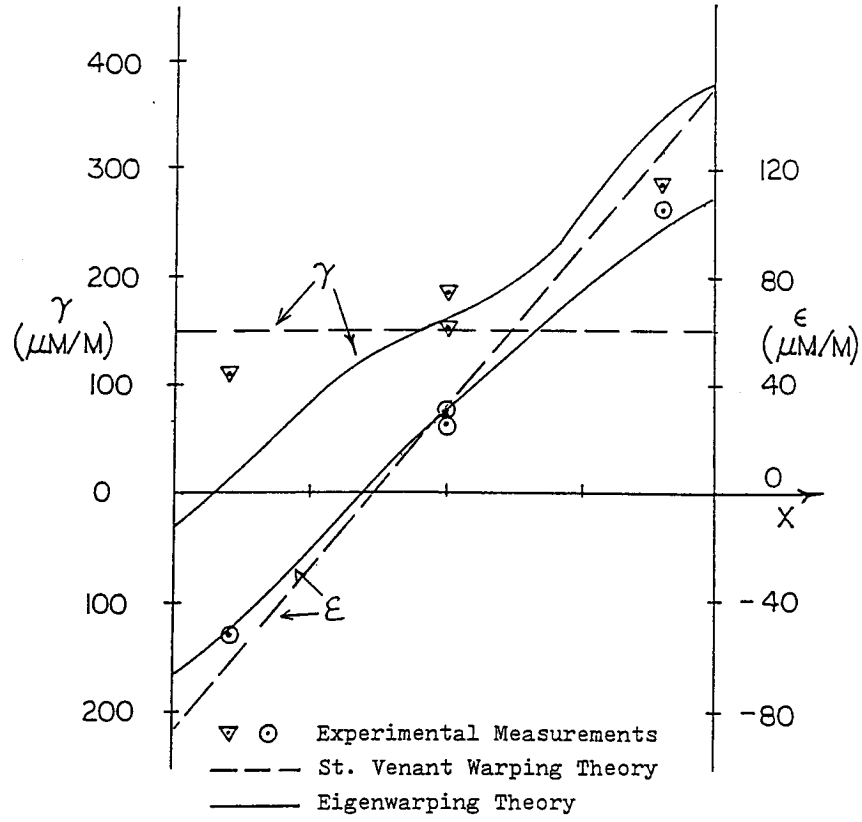

Figure 5. *Strain distributions in the upper skin of the unbalanced beam, at 45% span.*

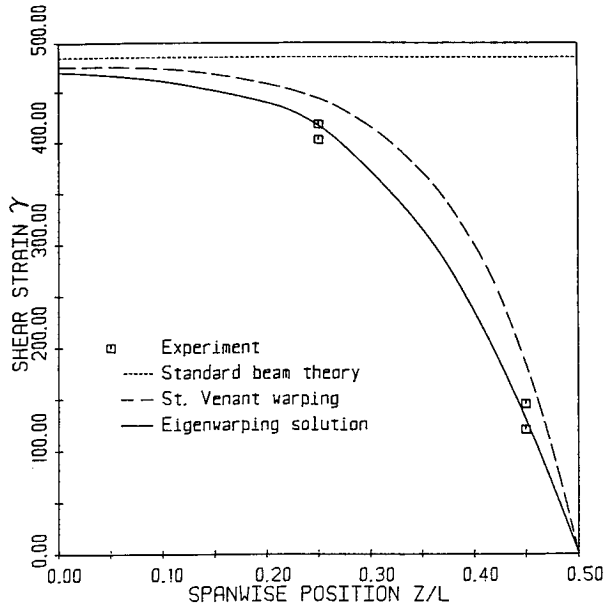

Figure 6. *Spanwise distributions of mid-width shearing strain, balanced beam configuration.*

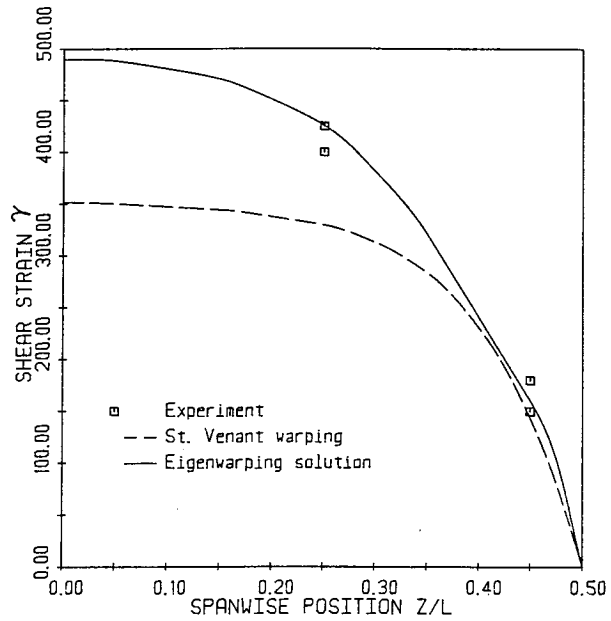

Figure 7. *Spanwise distributions of mid-width shearing strain, unbalanced beam configuration.*

ratio of the beam and the shearing modulus of the graphite/epoxy laminate were both rather low. Yet, the proposed analyses yield accurate predictions of the overall twist distribution of the beam. Similar axial strain distributions were found using the St. Venant warping and the Eigenwarping approaches, but the latter is more accurate in describing the shearing strain distribution. It is important to note the key role played by the warping deformation and warping constraint: these effects must be modeled carefully as they drastically influence the torsional behavior of composite beams. The elastic coupling behavior of thin-walled beams results from the shear-extension coupling term in the walls, A_{nq}. Careful handling of this term yields a consistent theory where all elastic couplings are accounted for.

The St. Venant warping and Eigenwarping approaches both provide consistent methodologies to model anisotropic beams where nonclassical influences such as warping deformation and warping constraints are important. Elastic couplings are dealt with in a rational fashion as well. Predicted twist and strain distributions are both in good agreement with experimental measurements.

ACKNOWLEDGEMENTS

The first two authors acknowledge the support of NASA and AFOSR under NASA Grant NGL 33-018-003. Dr. M. Greenfield and Dr. A. Amos are technical monitors in the respective agencies. The last author acknowledges ARO under Contract DAAG 29-82-K-0094. Dr. Robert Singleton and Dr. Gary Anderson are contract monitors.

REFERENCES

1. Tsai, S. W. and Hahn. *Introduction to Composite Materials*. Technomic Publishing Co. (1980).
2. Timoshenko, S. P. and J. N. Goodier. *Theory of Elasticity*. Mc-Graw-Hill Book Co. (1970).
3. Rehfield, L. W. "Design Analysis Methodology for Composite Rotor Blades," *Proceedings of the Seventh DOD/NASA Conference on Fibrous Composites in Structural Design, AFWAL-TR-85-3094, June 1985*, pp. (V(a)-1)-(V(a)-15).
4. Bauchau, O. A. "A Beam Theory for Anisotropic Materials," *J. Appl. Mech.*, 52:416–422 (June 1985).